

## A Comparative Molecular Field Analysis Study of *N*-Benzylpiperidines as Acetylcholinesterase Inhibitors

Weida Tong, Elizabeth R. Collantes, Yu Chen, and William J. Welsh\*

Department of Chemistry and Center for Molecular Electronics, University of Missouri—St. Louis, 8001 Natural Bridge Road, St. Louis, Missouri 63121

Received September 25, 1995<sup>©</sup>

A series of 1-benzyl-4-[2-(*N*-benzoylamino)ethyl]piperidine derivatives and of *N*-benzylpiperidine benzisoxazoles has been investigated using the comparative molecular field analysis (CoMFA) approach. These compounds have been found to inhibit the metabolic breakdown of the neurotransmitter acetylcholine (ACh) by the enzyme acetylcholinesterase (AChE) and hence alleviate memory deficits in patients with Alzheimer's Disease by potentiating cholinergic transmission. Development of the CoMFA model considered two separate alignments: (i) alignment I which emphasized the electrostatic fitting of the subject compounds and (ii) alignment II which emphasized their steric fitting. In addition, the inhibitor compounds were considered both as neutral species and as *N*-piperidine-protonated species. The resulting 3D-QSAR indicates a strong correlation between the inhibitory activity of these *N*-benzylpiperidines and the steric and electronic factors which modulate their biochemical activity. A CoMFA model with considerable predictive ability was obtained.

### Introduction

According to the cholinergic hypothesis, memory impairments in patients with senile dementia of the Alzheimer's type (SDAT) result from a deficit of cholinergic functions in the brain.<sup>1</sup> Progressive memory dysfunction in SDAT is associated with a decreased rate of formation of acetylcholine (ACh). One promising therapeutic strategy for activating central cholinergic functions has been the use of inhibitors of acetylcholinesterase (AChE), the enzyme responsible for the metabolic hydrolysis of ACh. Clinical studies with such AChE inhibitors have demonstrated positive results in terms of enhancing memory in patients with SDAT and related disorders.<sup>2</sup> The AChE inhibitor tacrine (1,2,3,4-tetrahydro-9-aminoacridine or THA) was approved by the U.S. Food and Drug Administration (FDA) in 1993 as the first and only treatment for SDAT in the United States.<sup>3</sup> Despite its wide usage, THA suffers from dose-limiting hepatotoxic complications, slow pharmacokinetics, and high incidence of side effects.<sup>4</sup> Physostigmine, a carbamate-type AChE inhibitor, has shown inconclusive results in clinical tests stemming from its short half-life and narrow therapeutic index.<sup>5</sup>

A novel family of AChE inhibitors, the *N*-benzylpiperidines, has exhibited superior efficacy both *in vitro* and *in vivo*, minimal side effects, fast pharmacokinetics, and high selectivity for AChE compared with THA and physostigmine.<sup>6,7</sup> The exceptional safety profile of the *N*-benzylpiperidines can be traced to their truly outstanding selectivity for AChE over butyrylcholinesterase (BuChE) as demonstrated by the BuChE/AChE ratios of IC<sub>50</sub> values in excess of 3000/1.<sup>7</sup> By comparison, THA and physostigmine show poor selectivity between AChE and BuChE. Clinical studies have shown that inhibition of BuChE, which is abundant in human plasma, may be associated with potentiating side effects.<sup>8</sup> Therefore, an inhibitor devoid of BuChE activity, such as the

*N*-benzylpiperidines, is likely to display higher therapeutic indices.

By virtue of their high specificity and potency, the *N*-benzylpiperidines have been the focus of several recent studies.<sup>6,7,9</sup> Their design, synthesis, and biological evaluation have been reported earlier by Sugimoto and co-workers<sup>6</sup> and have been further investigated by Villalobos et al.<sup>7</sup> While all of these AChE inhibitors belong to the same class of compounds, those reported by Villalobos et al.<sup>7</sup> contain the benzisoxazole heterocycle which was identified as a suitable bioisosteric replacement for the benzoyl moiety present in the compounds reported by Sugimoto and co-workers.<sup>6</sup> Structure–activity studies of this class of inhibitors have provided information regarding structural features that contribute to enhanced AChE inhibition. Such studies have indicated that both the benzoyl-containing functionality and the *N*-benzylpiperidine moiety are key features for binding and inhibition of AChE.<sup>6</sup>

To obtain further insight into the relationship between the structure and biological activity of these *N*-benzylpiperidines as AChE inhibitors, we have carried out quantitative structure–activity relationship (QSAR) studies using the Comparative Molecular Field Analysis (CoMFA) method introduced by Cramer et al.<sup>10</sup> in 1988. The CoMFA methodology of 3D-QSAR is based on the assumption that the interaction between an inhibitor and the enzyme is primarily noncovalent in nature and shape-dependent. By sampling the steric and electrostatic fields surrounding a set of inhibitors and correlating differences in those fields to biological activity, a QSAR can be derived. The inhibitory activities for this set of *N*-benzylpiperidines under study have already been measured experimentally,<sup>6,7</sup> but structural data on the AChE–inhibitor complexes are absent. Stimulated by this need for structure–activity relationships, the present work was undertaken to investigate the utility of CoMFA as a quantitative tool for describing inhibitory activities. It was therefore hoped that CoMFA can help delineate the structural prerequisites for enhanced binding to AChE and thus guide the rational

\* To whom correspondence should be addressed.

<sup>©</sup> Abstract published in *Advance ACS Abstracts*, January 1, 1996.

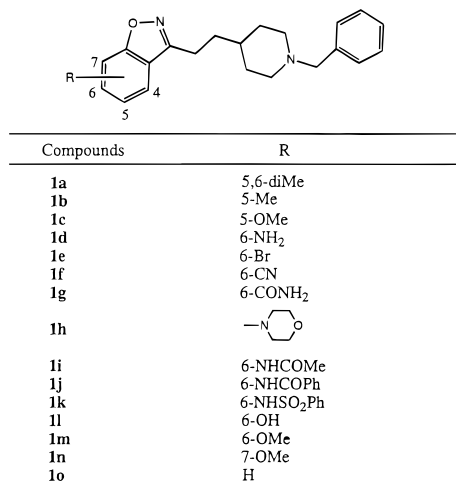


**Figure 1.** Benzisoxazole derivatives for AChE training set (from ref 7).

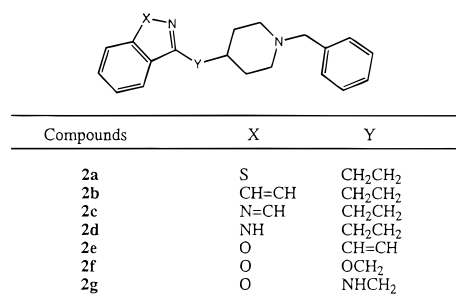


**Figure 2.** Benzisoxazole derivatives for the AChE training set (from ref 7).

design of the *N*-benzylpiperidine class of inhibitors for the palliative treatment of SDAT and related disorders associated with memory loss.

## Materials and Methods

**Data Set for Analysis.** Published *in vitro* biological data on a series of *N*-benzylpiperidine benzisoxazoles (NBPBs)<sup>7</sup> and of 1-benzyl-4-[2-(*N*-benzoylamino)ethyl]piperidine derivatives (NBEPs)<sup>6</sup> were used for this study. The structures of the 57 molecules constituting the training set in the QSAR analyses are found in Figures 1–5. In addition to the basic structural differences between the two sets of compounds involving the benzoyl bioisostere, the *N*-benzylpiperidines included in the model development differ from one another in several other respects, including (i) the substituents R on the benzisoxazole and/or benzoyl moieties, (ii) the length and nature of the aliphatic spacer group, and (iii) the substituents on the *N*-benzyl group.

The test set of compounds (Figure 6) included several derivatives drawn from compounds that were synthesized together with the above training set, as well as a series of rigid analogues that were later reported by Sugimoto et al.<sup>9</sup> In addition to several derivatives of E2020,<sup>11</sup> the test set also included THA and physostigmine to evaluate whether the CoMFA model applied to these two recognized AChE inhibitors.

**Computational Approaches.** All molecular modeling techniques and CoMFA studies described herein were performed on Silicon Graphics workstations using the SYBYL 6.1 molecular modeling software<sup>12</sup> from Tripos, Inc., St. Louis, MO.

**Molecular Conformation and Alignment.** The compounds were built from fragments in the SYBYL database, with compound **1o** (Figure 1) serving as a starting structure for the NBPBs and compound **3a** (Figure 3) as that for the NBEPs. Each structure was fully geometry optimized using the standard Tripos molecular mechanics force field with a distance-dependent dielectric function and a 0.001 kcal/mol energy gradient convergence criterion. Partial atomic charges

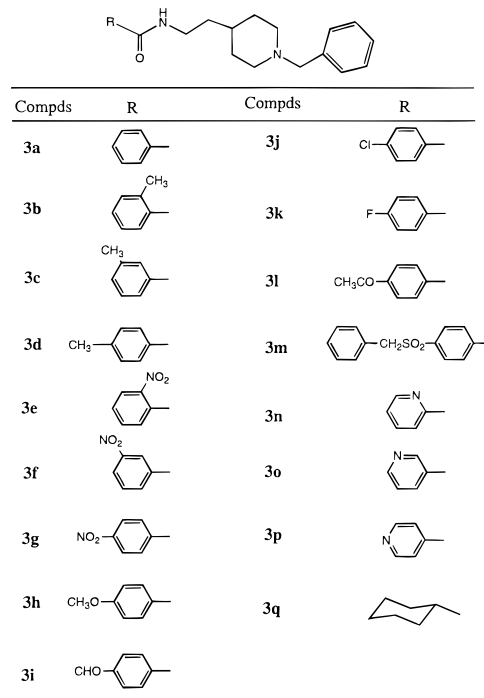


**Figure 3.** 1-Benzyl-4-[2-(*N*-(substituted-acyl)amino)ethyl]piperidine derivatives for the AChE training set (from ref 6).

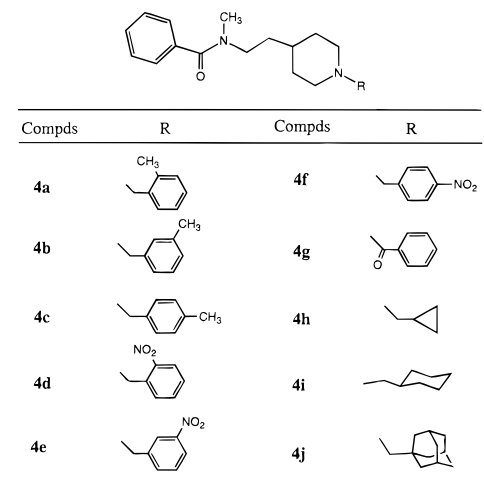


**Figure 4.** 1-Substituted-4-[2-(*N*-benzoyl-*N*-methylamino)ethyl]piperidine derivatives for the AChE training set (from ref 6).

required for calculation of the electrostatic interaction energies were calculated using the Gasteiger–Marsili method.<sup>13</sup>

These energy-minimized structures were then subjected to conformational analysis. Using the systematic search protocol, rotatable bonds affecting the disposition of the ethylene bridge and of the *N*-benzylpiperidine moiety were searched from 0 to 360° in 10° increments (Table 1). Each of the structures was then set to the minimum-energy torsion angle  $\phi$  and re-minimized. To ascertain whether these calculated geometries were reasonable, the Cambridge Structural Database (CSD)<sup>14</sup> was searched for (i) compounds possessing an ethylenic bridge and (ii) compounds with the *N*-benzylpiperidine moiety. An examination of the torsion angles obtained from the CSD search (Table 1) revealed that the torsion angle calculated for the ethylene bridge in the subject compounds is consistent with available crystallographic data on related compounds. In the same manner, the calculated torsion angles about the *N*-benzylpiperidine moiety compared well with crystallographic data on similar compounds. This comparison included **4g** and **4i** (Figure 4) for which the substituents are benzoyl and cyclohexyl, respectively.

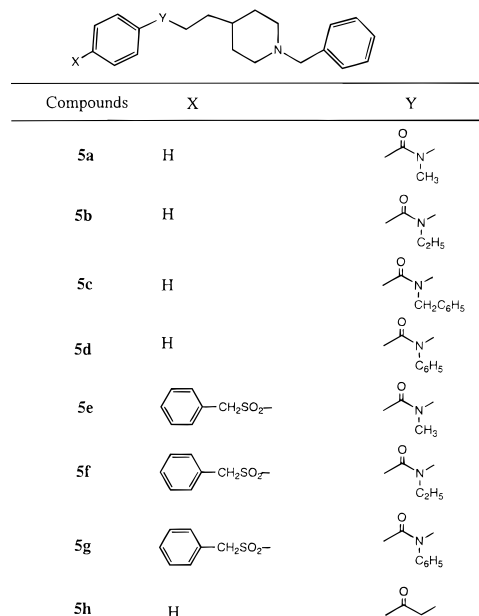


**Figure 5.** 1-Benzyl-4-[2-[*N*-(4'-substituted-benzoyl)-*N*-substituted-amino]ethyl]piperidine derivatives for the AChE training set (from ref 6).

The systematic search identified several local minimum-energy conformations for the NBPBs and NBEPs. This finding suggested several possible alignments relative to a template molecule. The use of multiple conformers in a CoMFA study has previously been reported.<sup>15</sup> For the NBPBs, the lowest energy conformation of each compound was selected. For the NBEPs, two separate low-energy conformations which differ with respect to torsion angle  $\phi_1$  (Table 1) were considered in generating the CoMFA model. With a representative NBPB conformer defined as the template molecule, the superimposition of these two conformers to the template NBPB therefore yielded two alignments designated I and II. In alignment I, the amide carbonyl present in NBEP compounds **3a–5h** was oriented toward the isoxazole oxygen of the NBPB template. In alignment II, this amide carbonyl is oriented in the opposite direction (i.e., away from the heteroatoms of the isoxazole moiety). For both alignments, the compounds were modeled in their neutral and *N*-piperidine-protonated forms.

CoMFA was then initiated using the minimum-energy conformations obtained as described above. As a first consideration, all molecules were in their neutral forms. The 6-morpholino analogue (**1h**) was chosen as the template molecule on which to align the various NBPB and NBEP analogues due to its superior potency and its high selectivity for AChE over BuChE.<sup>7</sup> For the NBPBs, the various compounds were aligned via root mean square (rms) fitting of atoms C4, C10, C12, N15, and C19 to the corresponding atoms of the **1h** template molecule (Table 1). The equivalent atoms for the NBEPs are C4, C9, C11, N14, and C18. These atoms were selected to consider the major regions of the *N*-benzylpiperidine skeletal structure, i.e., the phenyl group, the isoxazole or the amide group, the ethylene spacer, the piperidine ring, and the benzyl group. In choosing these particular atoms for the alignments, it was hoped to provide optimal fit among the compounds and, at the same time, minimal loss of conformational flexibility.

After the compounds were aligned using the rms fitting procedure described above, a field fit optimization to the template molecule was performed. The field fit adjusts the geometry of the molecules in order to obtain maximal similarity between the steric and electrostatic fields of template and training molecules. This operation sometimes produces structural distortions; subsequent reoptimization of the molecules would relax the fitted molecules to the nearest local minimum-energy structure.

Since the piperidine ring and non-amide nitrogens of the various inhibitors will likely be protonated at physiological pH, protons were added to the neutral structures for both align-

ments I and II. Torsion angles about the *N*-benzylpiperidine moiety were adjusted to match the values obtained from the CSD<sup>14</sup> for similarly protonated compounds (Table 1). These protonated molecules were subsequently reminimized and aligned as described above for the neutral analogues.

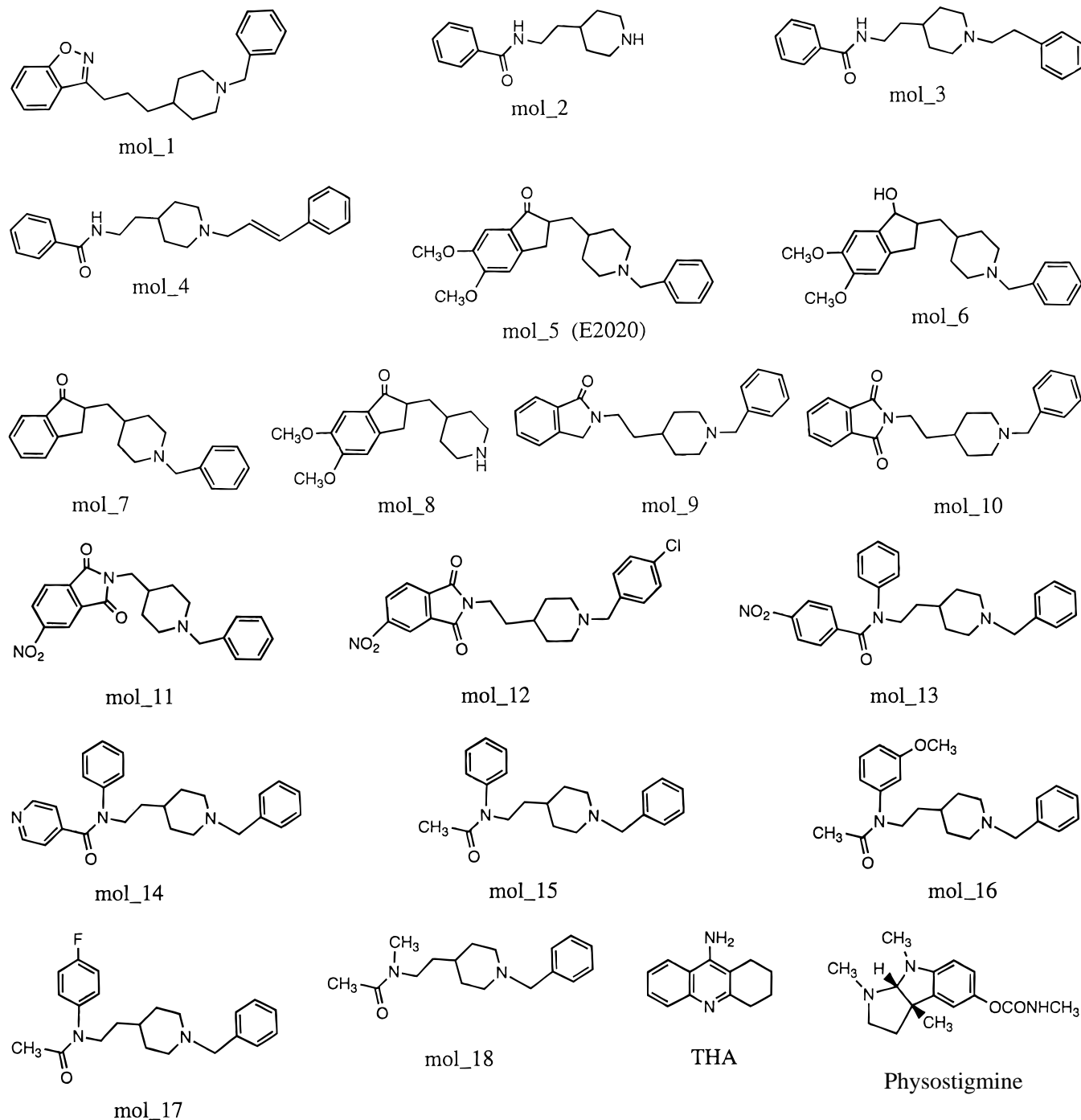
As in most studies dealing with conformationally flexible molecules, we have used the low-energy conformers for each molecule in the data set. The structural differences between the NBPBs and NPEBs allowed for some latitude in terms of choosing a specific alignment. On the basis of intuitive reasoning, the NPEBs and NBPBs were first aligned such that the amide carbonyl oxygen of the NPEBs nearly overlaid the benzisoxazole oxygen of the NBPBs. Designated alignment I, it presumes that the same hydrogen-bond donor in AChE (e.g., the backbone N-H of Phe-288 in AChE from *T. californica*)<sup>7</sup> binds the carbonyl oxygen in the NPEBs and the isoxazole oxygen in the NBPBs. The fitting provided by alignment I was deemed optimal for the electrostatics but not for the sterics among the NPEBs and NBPBs. An improved steric fit was attained by a rotation of 180° about  $\phi_1$  in NPEBs **3a–5h** (Table 1). Designated alignment II, it tacitly asserts that the loss in overlap of the hydrogen-bonding functionalities is offset by the gain in steric matching of the NBPBs and NPEBs. In effect, alignments I and II test the relative importance of sterics and electrostatics (i.e., hydrogen bonding) in the binding of the NPEBs to AChE. In the absence of experimental data on the precise binding modes of these inhibitors to AChE, both alignments should be considered plausible. By evaluating both alignments I and II, the present study provided an assessment of the sensitivity of CoMFA to the choice of alignment paradigm. Furthermore, CoMFA models for both alignments were developed and tested for this family of inhibitors separately as neutral species and as protonated species.

The compounds of the test set were prepared and modeled in a similar fashion to those of the training set, except that no field fit was performed. All test-set compounds were considered exclusively in their protonated forms inasmuch as they better match the normal substrate ACh which possesses the cationic quaternary nitrogen. The template molecule selected for alignment was either the 6-morpholino analogue (**1h**) or the training-set compound which most closely resembled the particular compound in question. In the case of THA and physostigmine, both contain a phenyl ring which was treated as a common feature with the benzisoxazole moiety of the 6-morpholino analogue (**1h**) as the template. Different superpositions of the phenyl ring relative to the template would orient the heteroatoms of THA and physostigmine either toward or away from the corresponding heteroatoms of the benzisoxazole. The optimal alignment was chosen based solely on the accuracy of prediction of inhibitory activity.

**CoMFA Interaction Energy Calculations.** For each of the alignment sets, the steric and Coulombic potential energy fields were separately calculated at each lattice intersection on a regularly spaced grid of 2.0 Å units in all *x*, *y*, and *z* directions. The steric term represents the van der Waals (6–12) interactions, while the Coulombic term represents the electrostatic interactions for which a distance-dependent dielectric expression  $\epsilon = \epsilon_0 R_{ij}$  with  $\epsilon_0 = 1.0$  was adopted. The grid pattern, generated automatically by the SYBYL/CoMFA routine, extended 5.0 Å units in all directions beyond the dimensions of each molecule. A CoMFA lattice with 1-Å grid spacing was also investigated, but the small improvement in the correlation did not justify the substantially increased computing time. Therefore, the default grid was adopted for all subsequent analyses.

An  $sp^3$  carbon atom with a van der Waals radius of 1.52 Å and a +1.0 charge was selected as the probe to calculate the steric and electrostatic fields. Values of the steric and electrostatic energy were truncated at 30 kcal/mol.

**Partial Least Squares (PLS) Analysis.** To obtain a 3D-QSAR, partial least squares<sup>16</sup> (PLS) fitting was used. The PLS method has been applied successfully in numerous QSAR studies aiming to rationalize those structural features affecting biological activity. PLS regression seeks a relationship between **Y** and **X**, where vector **Y** is the response or dependent variable and **X** represents the descriptor data.

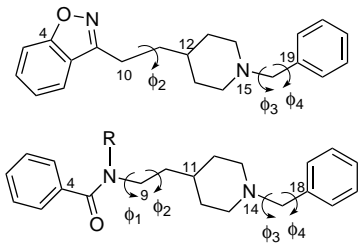


**Figure 6.** Structures of the compounds in the AChE test set (from refs 6, 7, 9, and 11).

The PLS algorithm was initially used with the cross-validation option to obtain the optimal number of components needed for the subsequent analysis of the data. In the leave-one-out cross-validation, each compound is systematically excluded from the set and its activity predicted by a model that is derived from the rest of the compounds. The optimal number of components is then chosen as that which yielded either the smallest rms error or the largest cross-validated  $r^2$  value. A final PLS analysis was then performed using the reported optimum number of components and with no cross-validation. This generated a fitted correlation of the entire training set with conventional  $r^2$  values. The steric and electrostatic fields were scaled according to CoMFA standard deviations in order to give them the same potential weights on the resulting QSAR. In most cases, including our own work, the use of COMFA\_STD scaling has been found to give better  $r^2$  values compared with those obtained using no scaling.<sup>12</sup> The 3D-QSAR calibration model so derived was then employed to predict the inhibitory values of the 20 compounds in the test set (Figure 6).

## Results and Discussion

**CoMFA of AChE Inhibitors.** The results of the CoMFA studies for the four training sets are summarized in Table 2. For alignment I, the CoMFA of the neutral molecules yielded a correlation with a cross-validated  $r^2$  of 0.616 and a conventional  $r^2$  of 0.912. An increase in the cross-validated (0.672) and conventional  $r^2$  (0.936) was obtained for the same set of compounds in their *N*-piperidine-protonated forms. It appears that the changes in steric and charge distributions concomitant with protonation resulted in a better alignment for the molecules in the data set. The correlation between calculated and experimental  $IC_{50}$  values (Table 3) for the protonated set of compounds is shown in Figure 7. This PLS regression analysis used six components for optimal fitting to explain the variance in the biological data. The relative contributions to the CoMFA model

**Table 1.** Values of Key Torsion Angles<sup>a</sup> Calculated by the Tripos Force Field Compared with Those Extracted from the Cambridge Structural Database (CSD) for Related Compounds


ref code	$\phi_2$	ref code	$\phi_3$	$\phi_4$	ref code	$\phi_3$	$\phi_4$
CEDZOA <sup>b</sup>	-175.6	Neutral Compounds			Protonated Compounds		
DTSOAR	-175.9	BOHJUD <sup>b</sup>	172.2	129.8	BZEPIP <sup>b</sup>	177.5	94.7
HFRUAC	-169.8	FEM LIS	174.2	129.4	BZETBH	161.0	90.4
<b>1j</b> <sup>c</sup>	-174.9	GIMYEG	168.2	115.6	CITHUI	167.1	69.4
<b>3a</b>	-171.5	TZSDCO	178.8	102.7	<b>1j</b> <sup>c</sup>	175.9	103.2
		<b>1j</b> <sup>c</sup>	165.7	135.1	<b>3a</b>	175.5	99.3
		<b>3a</b>	164.9	134.5			
					HADBIX	-56.0	-49.0
		BUTPOV	-171.9	-134.0	<b>4i</b>	-62.9	-40.5
		PNBPIP	-170.6	-134.1			
		<b>4g</b>	-171.2	-126.4			

<sup>a</sup> In units of degrees. <sup>b</sup> Each CSD structure is identified by its six-letter reference code. <sup>c</sup> Torsion angles for *N*-benzylpiperidines **1j**, **3a**, **4g**, and **4i** were calculated by Tripos force field.

**Table 2.** Summary of CoMFA-PLS Results for Training Set of 57 AChE Inhibitors

	alignment I		alignment II	
	neutral	protonated	neutral	protonated
$r^2_{\text{cross-validated}}$	0.616	0.672	0.635	0.722
$r^2_{\text{conventional}}$	0.912	0.936	0.850	0.962
std error	0.369	0.316	0.477	0.245
no. of components	5	6	4	6
<i>F</i> value	105.278	122.875	73.575	210.581
contributions				
steric	0.516	0.735	0.485	0.767
electrostatic	0.484	0.265	0.515	0.233

are 73.5% steric and 26.5% electrostatic, indicating that the variation in activity among the inhibitors is dominated by differences in steric (van der Waals) interactions with the AChE binding site.

For both alignments I and II, better cross-validated and conventional  $r^2$  values were obtained for the protonated compounds compared with the neutral compounds. For both neutral and protonated sets of compounds, alignment II yielded only a slight improvement in cross-validated and conventional  $r^2$  values compared with alignment I. Thus, CoMFA can formulate a 3D-QSAR equally well for the NPEBs when they are aligned to optimize electrostatic fit (alignment I) as when they are aligned to optimize steric fit (alignment II). Since the active site gorge in AChE is so deep and its aromatic surface so extensive, it has been postulated that several unique binding sites may be available for substrates and inhibitors.<sup>17</sup> Still, no conclusive determination regarding the precise binding mode of these *N*-benzylpiperidines, and particularly the NPEBs, can be made based on the present CoMFA results. As pointed out by Klebe and Abraham,<sup>18</sup> alignments constructed in the absence of experimental structural data on the binding mode(s) can deviate from the actual biologically active conformation since the aligning procedures do not explicitly account for entropic effects.

The NBPBs and NPEBs in the 57-compound training set actually constitute two distinct structural subsets within the same *N*-benzylpiperidine family. For this reason, a CoMFA was also performed separately for

**Table 3.** Observed versus Calculated IC<sub>50</sub> Values for Protonated Compounds in the Training Set for Models Based on Alignments I and II

compd	log IC <sub>50</sub> (obsd)	alignment I		alignment II	
		log IC <sub>50</sub> (calcd)	residual	log IC <sub>50</sub> (calcd)	residual
<b>1a</b>	0.763	1.04	-0.28	0.84	-0.08
<b>1b</b>	0.892	1.15	-0.26	0.90	-0.01
<b>1c</b>	0.857	0.94	-0.09	0.63	0.22
<b>1d</b>	1.301	1.56	-0.25	1.50	-0.20
<b>1e</b>	1.699	1.56	0.14	1.65	0.05
<b>1f</b>	2.004	1.55	0.46	1.52	0.49
<b>1g</b>	0.944	1.00	-0.06	0.85	0.10
<b>1h</b>	-0.097	-0.18	0.08	-0.13	0.04
<b>1i</b>	0.447	0.55	-0.10	0.54	-0.09
<b>1j</b>	0.973	0.82	0.16	0.87	0.10
<b>1k</b>	1.146	1.05	0.09	1.12	0.03
<b>1l</b>	1.415	1.51	-0.09	1.68	-0.27
<b>1m</b>	0.919	1.00	-0.08	0.98	-0.06
<b>1n</b>	0.851	0.71	0.14	1.15	-0.30
<b>1o</b>	1.740	1.69	0.05	1.51	0.23
<b>2a</b>	1.990	1.86	0.13	1.91	0.08
<b>2b</b>	2.342	2.19	0.16	2.24	0.10
<b>2c</b>	2.532	2.48	0.05	2.62	-0.09
<b>2d</b>	2.079	2.00	0.08	1.92	0.16
<b>2e</b>	2.322	2.27	0.05	2.67	-0.35
<b>2f</b>	3.412	3.11	0.31	3.58	-0.17
<b>2g</b>	2.505	2.67	-0.16	2.59	-0.08
<b>3a</b>	2.748	2.32	0.42	2.54	0.21
<b>3b</b>	3.000	2.94	0.06	2.79	0.21
<b>3c</b>	2.672	2.64	0.04	2.36	0.31
<b>3d</b>	2.255	2.15	0.11	2.02	0.23
<b>3e</b>	2.944	2.93	0.01	2.85	0.09
<b>3f</b>	2.362	2.32	0.04	2.54	-0.17
<b>3g</b>	1.740	1.81	-0.07	1.67	0.07
<b>3h</b>	1.944	1.94	0.01	2.03	-0.09
<b>3i</b>	2.079	2.04	0.03	2.19	-0.11
<b>3j</b>	2.255	2.07	0.18	2.19	0.06
<b>3k</b>	1.929	2.12	-0.19	2.27	-0.34
<b>3l</b>	1.708	1.56	0.15	1.46	0.25
<b>3m</b>	1.462	1.74	-0.28	1.80	-0.34
<b>3n</b>	2.903	2.44	0.46	2.76	0.14
<b>3o</b>	1.839	2.12	-0.28	1.81	0.03
<b>3p</b>	1.591	2.15	-0.56	2.07	-0.48
<b>3q</b>	3.204	3.14	0.06	3.13	0.08
<b>4a</b>	2.886	3.01	-0.13	2.96	-0.08
<b>4b</b>	2.161	2.49	-0.33	2.31	-0.15
<b>4c</b>	4.613	3.34	1.27	3.82	0.79
<b>4d</b>	4.146	3.81	0.33	3.75	0.40
<b>4e</b>	2.568	3.00	-0.43	2.85	-0.28
<b>4f</b>	3.518	3.11	0.41	3.61	-0.09
<b>4g</b>	4.716	4.70	0.02	4.56	0.16
<b>4h</b>	4.580	4.79	-0.21	4.73	-0.15
<b>4i</b>	2.613	2.68	-0.06	2.75	-0.14
<b>4j</b>	4.380	4.51	-0.13	4.33	0.05
<b>5a</b>	2.230	3.11	-0.88	2.76	-0.53
<b>5b</b>	2.114	2.33	-0.21	2.16	-0.05
<b>5c</b>	2.973	3.29	-0.32	3.07	-0.10
<b>5d</b>	1.544	1.44	0.11	1.70	-0.15
<b>5e</b>	-0.222	-0.11	-0.11	-0.19	-0.03
<b>5f</b>	-0.522	-0.74	0.22	-0.77	0.25
<b>5g</b>	-0.222	-0.17	-0.05	-0.23	0.01
<b>5h</b>	2.724	2.89	-0.17	2.71	0.02

each subset of compounds as protonated species using alignment I. The values of the cross-validated  $r^2$  and conventional  $r^2$  were 0.685 and 0.934, respectively, for the NPEBs and 0.653 and 0.986, respectively, for the NBPBs. These values compare well with the corresponding values 0.672 and 0.936 obtained above for the combination of the subsets (Table 2). This consistency suggests that each subset of compounds, considered apart from the other subset, provides adequate structure-activity information to construct a quality 3D-QSAR. At the same time, the high quality of the CoMFA model for the combination of subsets reinforces the fact that the NPEBs and NBPBs are members of

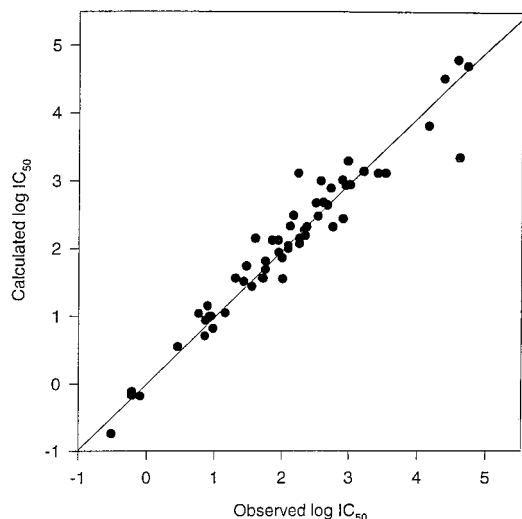


**Figure 7.** Plot of observed versus calculated log IC<sub>50</sub> values for training set compounds in alignment I.

the same family and likely bind AChE in identical or similar ways. Since it includes a more diverse set of structures in the training set and thereby provides a more robust regression, only the CoMFA model for the combination of subsets was considered in the subsequent analysis of the test set as discussed below.

**Prediction for Compounds of the Test Set.** The CoMFA models derived from the protonated compounds of alignments I and II were used to estimate the IC<sub>50</sub> values of the test compounds depicted in Figure 6. The analysis based on CoMFA steric and electrostatic fields yielded a predictive  $r^2$  of 0.817 for alignment I and 0.868 for alignment II. The predictive  $r^2$  refers only to molecules in the test set and was calculated as

$$\text{predictive } r^2 = (\text{SD} - \text{PRESS})/\text{SD}$$

where SD is the sum of squared deviations of each biological property value (log IC<sub>50</sub>) for each molecule in the test set from the mean of the training set and PRESS is the sum, over all molecules in the test set, of the squared differences between their actual and predicted biological property values.<sup>19</sup> Like the cross-validated  $r^2$ , the predictive  $r^2$  can assume a negative value reflecting a complete lack of predictive ability of the training set for the molecules included in the test set.<sup>20</sup>

The observed and corresponding CoMFA-predicted IC<sub>50</sub> values for the test-set compounds are listed in Table 4 and plotted in Figure 8. Comparison of these IC<sub>50</sub> values shows that CoMFA can generally predict the activity of new compounds to within a log unit of their measured value, regardless of whether they are active or inactive analogues. As expected, the model was highly predictive for all *N*-benzylpiperidine derivatives in the test set, thus reflecting the structural composition of the training set. The model also satisfactorily predicted the activity of several test-set compounds not represented in the training set. Consistent with the biological data, it predicted that **mol\_1** with a three-atom bridge and both **mol\_3** and **mol\_4** with extended substituents attached to the piperidine nitrogen are less active than **3a**. The model also satisfactorily predicted the activities for E2020 (**mol\_5**) and its derivatives **mol\_6** through **mol\_8** as well as for 1-benzyl-4-(2-phthalimidoethyl)piperidine and related structures **mol\_9**

**Table 4.** Observed versus Predicted IC<sub>50</sub> Values for Protonated Compounds in the Test Set for Models Based on Alignments I and II

compd	log IC <sub>50</sub> (obsd)	alignment I		alignment II	
		log IC <sub>50</sub> (pred)	residuals	log IC <sub>50</sub> (pred)	residuals
<b>mol_1</b>	2.954	2.657	0.297	2.376	0.578
<b>mol_2</b>	4.415	4.060	0.355	4.052	0.363
<b>mol_3</b>	4.114	4.726	-0.612	4.240	-0.126
<b>mol_4</b>	4.732	4.134	0.598	4.042	0.690
<b>mol_5</b>	0.903	1.892	-0.989	1.731	-0.828
<b>mol_6</b>	2.477	1.949	0.528	2.516	-0.039
<b>mol_7</b>	2.176	2.576	-0.400	2.551	-0.375
<b>mol_8</b>	3.732	3.676	0.056	3.954	-0.222
<b>mol_9</b>	1.991	1.935	0.056	2.368	-0.377
<b>mol_10</b>	1.477	1.980	-0.503	2.200	-0.723
<b>mol_11</b>	3.477	2.754	0.723	3.339	0.138
<b>mol_12</b>	2.380	1.553	0.827	1.886	0.494
<b>mol_13</b>	0.732	0.770	-0.038	0.998	-0.226
<b>mol_14</b>	1.806	1.245	0.561	1.392	0.414
<b>mol_15</b>	1.716	1.677	0.039	1.897	-0.181
<b>mol_16</b>	1.663	1.913	-0.250	2.000	-0.337
<b>mol_17</b>	2.312	1.765	0.547	1.887	0.425
<b>mol_18</b>	2.819	2.904	-0.085	2.331	0.483
THA	2.431	2.640	-0.209	4.940	-2.509
physostigmine	1.278	1.978	-0.700	2.850	-1.572

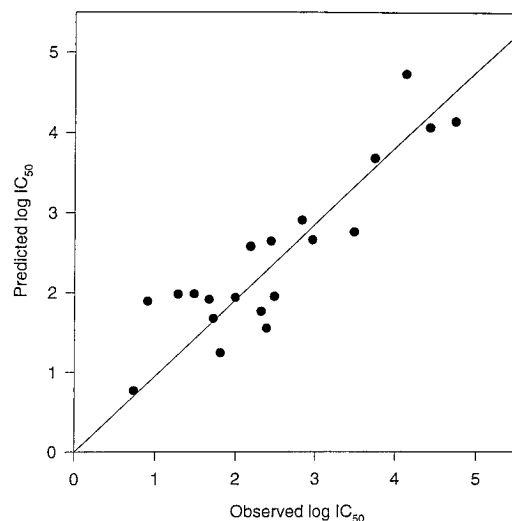


**Figure 8.** Plot of observed versus predicted log IC<sub>50</sub> values for test set compounds in alignment I.

through **mol\_18**. Of particular note, the model performed reasonably well in predicting the activity of THA and, to a lesser degree, physostigmine. These latter two AChE inhibitors are quite distinct from the compounds in the training set (Figures 1–5) in terms of both chemical structure and, presumably, mode of binding.<sup>21</sup> This suggests that THA, which belongs to the aminoacridine family of inhibitors, and physostigmine, which is a carbamate ester type of inhibitor, fall within the spatial bounds of the 3D-QSAR CoMFA model although not apparent from a 2D perspective. The impressive results obtained for these test-set compounds provides compelling evidence that the CoMFA model so derived is predictive for structurally diverse classes of compounds.

**CoMFA Fields.** In order to visualize the information content of the derived 3D-QSAR model, CoMFA contour maps were generated by interpolating the products between the 3D-QSAR coefficients and their associated standard deviations. Figure 9 shows a stereoview of the CoMFA steric contour map from the analysis based on alignment I using compounds **1j** and **3a** as reference structures. The green and yellow polyhedra describe

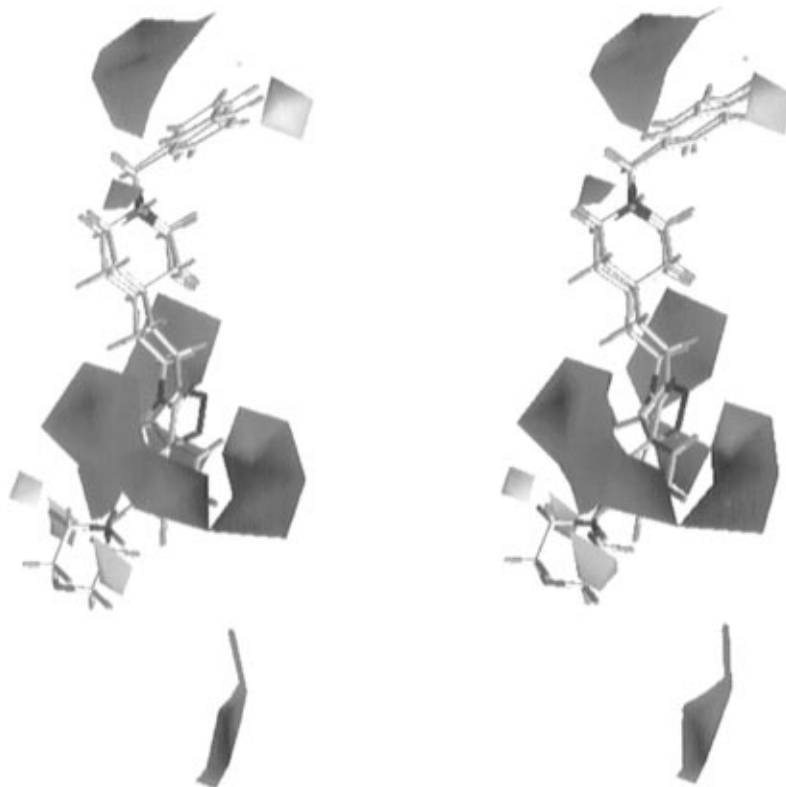


**Figure 9.** Stereoview of the CoMFA steric contour plot from the PLS analysis based on alignment I. Regions where increased steric bulk is associated with enhanced activity are indicated in green, while regions where increased steric bulk is associated with diminished activity are indicated in yellow.

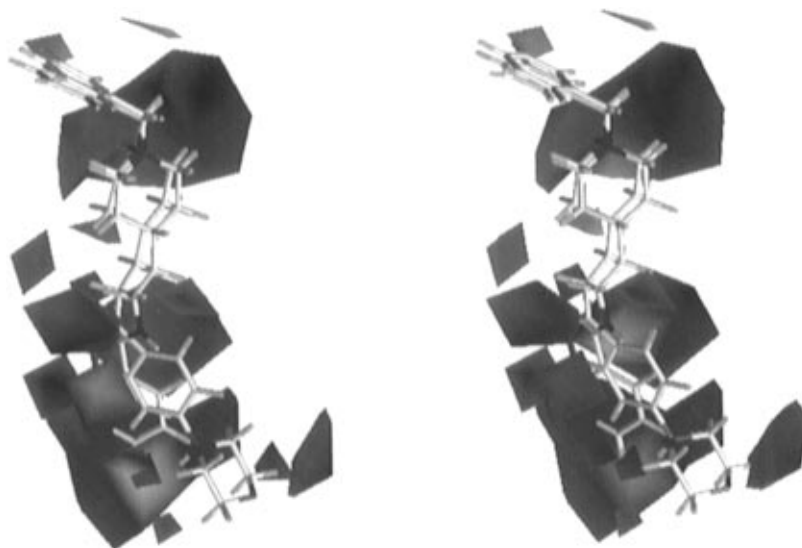


**Figure 10.** Stereoview of the CoMFA electrostatic contour plot from the PLS analysis based on alignment I. Regions where increased positive charge is favorable for activity are indicated in blue, while regions where increased negative charge is favorable for activity are indicated in red.

regions of space around the molecules where increases in steric bulk respectively enhance or diminish inhibition of AChE. An examination of the CoMFA steric field is consistent with the known SAR. Placing bulky and/or lipophilic groups at the benzisoxazole and benzoyl moieties is predicted to enhance the inhibitory effect on AChE. Hence, enhanced activity is shown for analogues **1j** with R = 6-morpholino and **1g** with R = 6-NHAc substituents and for analogues **5e–g** where the benzylsulfonyl group is in the para position. Consistent with this assessment, green contours in the CoMFA steric map surround the immediate portion of these substituents. The steric field map also indicated that occupying the ortho position of the benzoyl moiety with

steric bulk has a measurable negative effect on activity as represented by the diminished activities of **3b** and **3e** and of the NBPBs with substituents in the 5-position. The presence of yellow polyhedra in the area of the benzyl ring of *N*-piperidine is also noted, i.e., activity would be favored by substituents such as CH<sub>3</sub> but not NO<sub>2</sub>.

Figure 10 shows a stereoview of the same structures embedded in the CoMFA electrostatic contour maps. The red and blue polyhedra describe regions where a high electron density (i.e., negative charge or polarity) within the substrate structure enhances or diminishes activity, respectively. It can be seen that the red contour surrounds the oxygen of the isoxazole ring.

Hence, replacing the more electronegative oxygen with sulfur (**2a**) or nitrogen (**2d**) is predicted to diminish potency. The region corresponding to the piperidine region has been implicated as contributing substantially to AChE inhibition.<sup>7</sup> The presence of the red contour near the *N*-piperidine reinforces the importance of the basicity of the nitrogen atom in contributing to activity. Presumably, this contour also describes the negative effect on potency caused by electron-withdrawing groups on the benzyl group as represented by **4g**. Similarly, positive charge near the 2- and 3-positions would favor enhanced activity.

## Concluding Remarks

The CoMFA method has been applied successfully to rationalize the anti-AChE activity of a novel class of 57 inhibitors in terms of their steric and electrostatic properties. This model was developed from alignment strategies based upon reasonable assumptions for the binding modes for this family of *N*-benzylpiperidines. The 3D-QSAR culminating from the training set yielded a regression equation with a high degree of statistical significance and performed exceptionally well in predicting the biological activity (IC<sub>50</sub>) of most compounds in the test set, even those (e.g. THA) not represented in the training set. However, it must be emphasized that the two alignments (I and II) considered in this study were selected in the absence of experimental structural data on the AChE-inhibitor complex for these compounds. While awaiting the availability of such experimental information, we have initiated a set of tandem Monte Carlo-molecular dynamics simulations on the AChE-inhibitor complexes for these *N*-benzylpiperidines in order to validate and refine our current alignment strategies. These simulations are made possible by the availability of the X-ray crystallographic coordinates of AChE from *Torpedo californica*<sup>17,21</sup> bound to ACh. In subsequent CoMFA studies, we will expand our QSAR model to include other regressors such as AChE-inhibitor binding energies, the number and strength of hydrogen bonds, and hydrophobicity indices.

**Acknowledgment.** The authors wish to acknowledge Dr. James Blake of Pfizer, Inc., Groton, CT, for his collaboration in this study. The authors also acknowledge the financial support provided by the State of Missouri Alzheimer's Disease and Related Disorders Program Advisory Board and by the University of Missouri-St. Louis Center for Molecular Electronics. Finally, the authors wish to thank Tripos Associates, Inc., for access to their molecular modeling program Sybyl and in particular CoMFA.

## References

- (1) (a) Perry, E. K. The Cholinergic Hypothesis – Ten Years on. *Br. Med. Bull.* **1986**, *42*, 63–69. (b) Bartus, R. T.; Dean, L. D., III; Beer, B.; Lippa, A. S. The Cholinergic Hypothesis of Geriatric Memory Dysfunction. *Science* **1982**, *217*, 408–417.

- (2) Kumar, V.; Calache, M. Treatment of Alzheimer's Disease with Cholinergic Drugs. *Int. J. Clin. Pharmacol., Ther. Toxicol.* **1991**, *29*, 23–37.
- (3) *Scrip* **1993**, 1856, 19.
- (4) Farlow, M.; Gracon, S. I.; Hershey, L. A.; Lewis, K. W.; Sadowsky, C. H.; Dolan-Ureno, J. A. Controlled Trial of Tacrine in Alzheimer's Disease. *J. Am. Med. Assoc.* **1992**, *268*, 2523–2529.
- (5) Giacobini, E.; Somani, S.; McIlhenny, M.; Downen, M.; Hallak, M. Pharmacokinetics and Pharmacodynamics of Physostigmine after I.V. Administration in Beagle Dogs. *Neuropharmacology* **1987**, *26*, 831–836.
- (6) Sugimoto, H.; Tsuchiya, Y.; Sugumi, H.; Higurashi, K.; Karibe, N.; Iimura, Y.; Sasaki, A.; Kawakami, Y.; Nakamura, T.; Araki, S.; Yamanishi, Y.; Yamatsu, K. Novel Piperidine Derivatives. Synthesis and Anti-Acetylcholinesterase Activity of 1-Benzyl-4-[2-(*N*-benzoylamino)ethyl]piperidine Derivatives. *J. Med. Chem.* **1990**, *33*, 1880–1887.
- (7) Villalobos, A.; Blake, J. F.; Biggers, C. K.; Butler, T. W.; Chapin, D. S.; Chen, Y. P. L.; Ives, J. L.; Jones, S. B.; Liston, D. R.; Nagel, A. A.; Nason, D. M.; Nielsen, J. A.; Shalaby, I. A.; White, W. F. Novel Benzisoxazole Derivatives as Potent and Selective Inhibitors of Acetylcholinesterase. *J. Med. Chem.* **1994**, *37*, 2721–2734.
- (8) Thomsen, T.; Zende, B.; Fischer, J. P.; Kewitz, H. In Vitro Effects of Various Cholinesterase Inhibitors on Acetyl- and Butyrylcholinesterase of Healthy Volunteers. *Biochem. Pharmacol.* **1991**, *41*, 139–141.
- (9) Sugimoto, H.; Tsuchiya, Y.; Sugumi, H.; Higurashi, K.; Karibe, N.; Iimura, Y.; Sasaki, A.; Araki, S.; Yamanishi, Y.; Yamatsu, K. Synthesis and Structure-Activity Relationships of Acetylcholinesterase Inhibitors: 1-Benzyl-4-(2-phthalimidoethyl)piperidine and Related Derivatives. *J. Med. Chem.* **1992**, *35*, 4542–4548.
- (10) Cramer, R. D., III; Patterson, D. E.; Bunce, J. D. Comparative Molecular Field Analysis (CoMFA). 1. Effect of Shape on Binding of Steroids to Carrier Proteins. *J. Med. Chem.* **1988**, *110*, 5959–5967.
- (11) Pang, Y.-P.; Kozikowski, A. P. Prediction of the Binding Site of 1-benzyl-4-[(5,6-dimethoxy-1-indanon-2-yl)methyl]piperidine in Acetylcholinesterase by Docking Studies with the SYSDOC Program. *J. Comput.-Aided Mol. Des.* **1994**, *8*, 683–693.
- (12) SYBYL Molecular Modeling System, Version 6.1; Tripos, Inc., St. Louis, MO 63144.
- (13) Gasteiger, J.; Marsili, M. Iterative Partial Equalization of Orbital Electronegativity: a Rapid Access to Atomic Charges. *Tetrahedron* **1980**, *36*, 3219–3228.
- (14) Cambridge Structural Database, University Chemical Laboratory, Lensfield Rd., Cambridge CB2 1EW, England.
- (15) Nicklaus, M. C.; Milne, G. W.; Burke, T. R. QSAR of Conformationally Flexible Molecules: Comparative Molecular Field Analysis of Protein-Tyrosine Kinase Inhibitors. *J. Comput.-Aided Mol. Des.* **1992**, *6*, 487–504.
- (16) Wold, S.; Albano, C.; Dunn, W. J., III; Edlund, U.; Esbensen, K.; Geladi, P.; Hellberg, S.; Johansson, E.; Lindberg, W.; Sjostrom, M. Multivariate Data Analysis in Chemistry. In *Chemometrics: Mathematics and Statistics in Chemistry*; Kowalski, B., Ed.; Reidel: Dordrecht, The Netherlands, 1984.
- (17) Sussman, J. L.; Harel, M.; Frolow, F.; Oefner, C.; Goldman, A.; Toker, L.; Silman, I. Atomic Structure of Acetylcholinesterase from *Torpedo californica*: A Prototypic Acetylcholine-Binding Protein. *Science* **1991**, *253*, 872–879.
- (18) Klebe, G.; Abraham, U. On the Prediction of Binding Properties of Drug Molecules by Comparative Molecular Field Analysis. *J. Med. Chem.* **1993**, *36*, 70–80.
- (19) Waller, C. L.; Oprea, T. I.; Giolitti, A.; Marshall, G. R. Three-Dimensional QSAR of Human Immunodeficiency Virus (I) Protease Inhibitors. 1. A CoMFA Study Employing Experimentally-Determined Alignment Rules. *J. Med. Chem.* **1993**, *36*, 4152–4160.
- (20) Cramer, R. D., III; Bunce, J. D.; Patterson, D. E. Crossvalidation, Bootstrapping, and Partial Least Squares Compared with Multiple Regression in Conventional QSAR Studies. *Quant. Struct.-Act. Relat.* **1988**, *7*, 18–25.
- (21) Harel, M.; Schalk, I.; Ehret-Sabatier, L.; Boulet, F.; Goeldner, M.; Hirth, C.; Axelsen, P. H.; Silman, I.; Sussman, J. L. Quaternary Ligand Binding to Aromatic Residues in the Active-Site Gorge of Acetylcholinesterase. *Proc. Natl. Acad. Sci. U.S.A.* **1993**, *90*, 9031–9035.

JM950704X